Applied Catalysis B: Environmental 240 (2019) 182–192

Contents lists available at ScienceDirect

Applied Catalysis B: Environmental

journal homepage: www.elsevier.com/locate/apcatb

Dehydration of sorbitol to isosorbide over hydrophobic polymer-based solid acid

Danping Yuan[a,b], Ning Zhao[a], Yanxia Wang[a,b], Keng Xuan[a,b], Feng Li[a], Yanfeng Pu[a], Feng Wang[a], Lei Li[a,*], Fukui Xiao[a,*]

[a] State Key Laboratory of Coal Conversion, Institute of Coal Chemistry, Chinese Academy of Sciences, Taiyuan 030001, PR China
[b] University of Chinese Academy of Sciences, Beijing 100049, PR China

ARTICLE INFO

Keywords:
Sorbitol
Isosorbide
Dehydration
Polymer-based solid acid
Hydrophobicity

ABSTRACT

A series of hydrophobic polymer-based solid acid catalysts PDS (x) were synthesized via hydrothermal synthesis method of sodium p-styrenesulfonate hydrate (SPSS) and divinylbenzene (DVB), followed by ion exchange. The specific surface area, acid sites concentration and hydrophobicity of the catalyst can be controlled by changing the amount of sodium styrene sulfonate, and the molar ration of SPSS and DVB from 0 to 0.4. Characterization results show that the PDS (x) catalysts have mesoporous structure (9.07–10.82 nm), large surface area (635–1039 m^2/g), rich acidic sites (0.25–1.72 mmol/g), high thermal stability and super hydrophobicity. Assessed in the dehydration reaction of sorbitol to isosorbide, the catalyst shows a remarkable catalytic performance when the molar ratio of SPSS to DVB is 0.3, yielding up to 81.7%, at 150 °C, which is equivalent that of H_2SO_4. The catalyst can be recycled five times with no significant decrease in activity. The superior performance can be attributed to the unique polymer network and acidic property.

1. Introduction

The rapid depletion of fossil resources that lead to emissions of carbon dioxide, has prompted the conversion of biomass to be an important research direction [1]. Terrestrial lignocellulose resources composed of polysaccharides are essential low cost feedstock for biorefineries which is capable of producing cellulose (C_6 sugars) and hemicellulose (C_5 sugars) via depolymerization [2]. Sorbitol can be obtained by hydrolysis and hydrogenation of abundance and cheap lignocellulose or glucose [3,4], which is then the top 10 building block chemical both in DOE's (the US Department of Energy) 2004 report [5] and in the update list of chemicals derived from bio-based products [6].

Sorbitol is discussed as a useful chemical, as it could be employed to produce a series of value-added bio-based chemicals and materials through dehydration, hydrogenolysis, polymerization and other reactions. Among which the double dehydration products, isosorbide, could be convert into polymer, functional material, solvent of cosmetics, pharmaceutical molecules, surfactants, plasticizers, food additives and even as a fuel or fuel additive [7,8]. Hence, isosorbide is considered as a high-value platform compound to replace fossil resources.

Based on the reaction mechanism, the conversion of sorbitol proceeds via the intramolecular S_N2-type reaction over acidic catalysts [9]. Traditional isosorbide production uses homogeneous acid as catalyst, including Brønsted acids (sulfuric acid, hydrochloric acid, phosphoric acid, etc.) and Lewis acids (metal chlorides/metal sulfonates) [10–14]. As early as 1930, sulfuric acid was firstly applied as the catalyst to obtain isosorbide [15]. Subsequently, other mineral acids, organic acids including H_2SO_4, HCl, H_3PO_4, p-toluenesulfonic acid and their mixtures [16,17] were investigated. Among them, H_2SO_4 showed the best activity and was widely used for the production of isosorbide in industry [18]. Despite the high activity, the homogeneous acid catalysts, suffered from the disadvantages of corrosion of equipment, difficult separation and regeneration. From the perspective of sustainable development and green chemistry, it is imminent to develop efficient and environmentally friendly heterogeneous catalysts to replace the homogeneous catalysts.

Dussenne et al. have summarized the synthetic strategies and catalysts development for isosorbide [19]. It was expected that Brønsted acid sites concentration and the textural properties would have a significant effect on the sorbitol dehydration reaction. Therefore, various solid acid catalysts, such as zeolites [20,21], supported metal oxides, metal phosphates, sulfated and phosphate metal oxides [22], supported HPA, Ru–Cu bimetals and acid resins are studied [23–25]. Among the zeolite catalysts, the H-Beta zeolite with silicon/aluminum ratio of 75

* Corresponding authors.
E-mail addresses: lilei@sxicc.ac.cn (L. Li), xiaofk@sxicc.ac.cn (F. Xiao).

https://doi.org/10.1016/j.apcatb.2018.08.036
Received 3 April 2018; Received in revised form 14 August 2018; Accepted 16 August 2018
Available online 30 August 2018

gives the best selectivity (127 °C, 2 h, 76%–80% yield of isosorbide) [26,27]. Li et al. found that the highest isosorbide yield (28%) was obtained at 250 °C under H_2 after 6 h over Ni/AC [28]. Gu et al. studied the effect of metal (IV) phosphates (tin, zirconium and titanium) on the reaction and found that tin phosphate shows the best catalytic activity (300 °C, 2 h, 47% yield of isosorbide) [29]. Metal (III) phosphates (Al-, Fe-, Ce-, La-) and metal (IV) phosphates (Zr-) are also studied, and the highest yield of isosorbide was 79.9% at 220 °C, 24 h [30]. Moreover, metal sulfonates and phosphates, such as $CuSO_4{\cdot}5H_2O$ (CuSO-650) (67% yield of isosorbide, 200 °C, 4 h) [31], sulfated zirconia (61% yield of isosorbide, 210 °C, 2 h) [32], sulfated titanium (75% yield of isosorbide, 210 °C, 2 h) [33], sulfated tin oxides (65% yield of isosorbide, 180 °C, 2 h) [34], phosphoric acid modified Nb_2O_5 (0.8 P/NBO-400) (62.5% yield of isosorbide, 225 °C, 5 h) [35] and tantalum oxides (0.8 P/TaO) (47% yield of isosorbide, 225 °C, 6 h) [36] are employed for the reaction. Furthermore, tungstophosphoric acids (PW) dispersed on metal oxides (SiO_2, γ-Al_2O_3, TiO_2, ZrO_2 and CeO_2) have been investigated over which 53% yield of isosorbide at 250 °C was obtained [37]. However, the high reaction temperature might lead to by-products and humins. Therefore, it is necessary to develop a green, cheap and efficient solid acid catalyst for dehydration of sorbitol at lower temperature.

Based on these considerations sulfonic acid resins [38], such as hydrophilic sulfonic acid functional silicon microspheres (SA-SiO_2) [39], Purolite [40], Amberlyst type resins [41], propyl sulfonic acid functionalized mesostructured SBA-15 silica [42], glucose derived magnetic solid acid (Glu-Fe_3O_4-SO_3H) [43], superhydrophobic mesoporous polymer-based acid catalyst (P-SO_3H) have been studied [44]. Among them, P-SO_3H with adjustable surface hydrophobicity, pore structure and the number of active sites shows prospect for the dehydration of sorbitol to isosorbide (87.9% yield of isosorbide) [44]. However, the effect of the catalysts on the dehydration reaction of sorbitol was not clarified.

Herein, we synthesized a cheap, efficient, environment-friendly, superhydrophobic mesoporous polymer-based solid acid catalyst (PDS (x)) via free radical copolymerization of SPSS and DVB. The acid sites concentration and the pore structure can be simultaneously adjusted by varying the amounts of sodium p-styrene sulfonate. The catalysts show superior activity and excellent recyclability for the sorbitol dehydration reaction under mild conditions. High specific surface area, mesoporous structure, superhydrophobicity and stabilized sulfonic acid groups might account for the excellent performance.

2. Experimental

2.1. Materials

Unless stated, all chemicals with AR (analytical reagent grade) in this work were purchased and used without further purification. D-sorbitol ($C_6H_{14}O_6$, 98%), isosorbide ($C_6H_{10}O_4$, 98%), 3,6-anhydro-D-galactose ($C_6H_{12}O_5$, ≥95%), 1,5-anhydro-D-glucitol ($C_6H_{12}O_5$), tetrahydrofuran (THF, 99%), 2, 2′-Azobis (2-methylpropionitrile) (AIBN, $C_8H_{12}N_4$, 99%) and sodium p-styrenesulfonate hydrate (SPSS, $C_8H_7NaO_3S{\cdot}xH_2O$, 90%) were purchased from Shanghai Aladdin Bio-Chem Technology Co., Ltd. 1,4-anhydro-sorbitol ($C_6H_{12}O_5$) was obtained from TRC Canada. 2,5-anhydro-D-glucitol ($C_6H_{12}O_5$) was obtained from J&K Chemical Ltd. Isomannide ($C_6H_{10}O_4$, > 97%) and galactitol ($C_6H_{14}O_6$, > 98%) were purchased from TCI (Shanghai) Development Co. Ltd. Ethanol absolute was purchased from Sinopharm Chemical Reagent Co. Ltd. Sodium hydroxide was purchased from Tianjin Hengxing Chemical Reagent. Sodium chloride and sulfuric acid (98%) were purchased from Tianjin Tianli Chemical Reagent. Divinylbenzene ($C_{10}H_{10}$, 80%) was purchased from Macklin Biochemical Co., Ltd. Amberlyst-15 was purchased from Acros Organics.

2.2. Catalyst preparation

2.2.1. PDVB-SO_3Na-x

Before synthesizing the mesoporous PDVB, polymerization inhibitor was removed from DVB as follows. Firstly, 10 mL of DVB containing polymerization inhibitor was washed by 500 mL of 5% sodium hydroxide solution in separating funnel at room temperature. Thereafter, the above DVB solution was washed with deionized water to pH = 7. Finally, the obtained DVB solution was used for polymerization. The hydrophobic polymer precursor PDVB-SO_3Na-x (where x stand for the initial molar ratio of SPSS and DVB) was prepared by free radical copolymerization of DVB and SPSS using AIBN as initiator under hydrothermal condition. The molar ratio of DVB/ SPSS/ AIBN/ THF/ H_2O was 1/x/ 0.02/ 16.1/ 7.23. Typically, 2 g DVB was dissolved in a solution containing 0.05 g AIBN, 20 mL THF and 2 mL deionized water. Then, 0.96 g SPSS was added. Upon stirring for 3 h at room temperature, the solution was transferred to the autoclave and heated to 100 °C for 24 h. After evaporation of solvents for 48 h at room temperature, the white bulk solid PDVB-SO_3Na-0.3 was obtained.

2.2.2. PDVB-SO_3H-x

PDVB-SO_3H-0.3 was synthesized by ion-exchange in 1 M aqueous solution of sulfuric acid and ethanol. In the typical synthesis, 1 g PDVB-SO_3Na-0.3 was added into 100 mL of 1 M sulfuric acid. After stirring for 24 h at room temperature, the sample was filtered and washed with large amount of deionized water until the filtrate was neutral. Then, the solid sample was dried at 80 °C for 10 h. The obtained sample was denoted as PDS (0.3). Other PDS (x) samples synthesis methods are similar to the above mentioned methods [45,46].

2.2.3. Catalyst characterization

The textural properties of the prepared samples were determined from the N_2 adsorption-desorption isotherms at liquid nitrogen temperature (−195.8 °C), using a Micromeritics Tristar II (3020) instrument (sample pretreatment: outgassing at 150 °C for 10 h under vacuum). The Brunauer-Emmett-Teller (BET) equation was used to analyze the specific surface areas and the Barrett-Joyner-Halenda (BJH) equation was used to calculate the pore volume.

The S content of catalysts was determined by CHN elemental analyses (EA) on Vario EL CUBE instrument and calculated by mass difference.

The number of acid sites was measured by acid-base titration. Firstly, the catalysts were ion-exchanged in 20 mL 2 M NaCl solution for 24 h, filtered, washed with 10 mL of deionized water, then the filtrate was titrated with standard NaOH solution.

The pyridine-adsorbing IR (Py-IR) spectra of PDS (x) catalysts were recorded on a Bruker Tensor 27 spectrometer at a resolution of 4 cm^{-1}. Before the measurements, selfsupported catalyst wafers (10 mg) were purged at 200 °C under vacuum for 2 h and the background was collected at 50 °C. Then pyridine vapour was introduced to the IR cell for 10 min after the sample was cooled to room temperature. Subsequently, the Py-IR spectra were collected after outgassing at 150 or 200 °C for 30 min.

Powder X-ray diffraction (XRD) analysis was collected on a Rigaku MiniFlex II desktop X-ray diffractometer, using Cu-Kα monochromatized radiation source at 30 kV and 15 mA from 5° to 85° with a scan rate of 4°/min.

Scanning electron microscopy (SEM) images were viewed on a JEOL JSM-7001 F (Japan) electron microscope with an acceleration voltage of 10 kV.

Transmission electron microscope (TEM) analysis was carried on a JEM-2100 F high resolution transmission electron microscopy operating at 200 kV.

The water contact angles (CA) were carried out on SL200B, Kino, America.

The adsorption isotherms of water were recorded at 25 °C on a

BELSORP-max instrument. Before measurement, a certain amount (≈25 mg) of sample was degassed at 150 °C for 10 h.

Fourier transform infrared spectroscopy (FT-IR) was recorded on a Nicolet Nexus 470 FT-IR Spectrometer over a range of 4000–400 cm^{-1} with 64 scans and a resolution of 2 cm^{-1}. The samples were diluted in KBr.

X-ray photoelectron spectroscopy (XPS) was conducted on the Thermo Fisher ESCALAB 250 xi equipped with Al Kα X-ray source (1486.6 eV).

Thermogravimetric analysis (TGA) was carried out with Rigaku Thermo plus Evo TG 8120 in a dry air atmosphere (30 mL/min) at a heating rate of 10 °C/min, from room temperature to 800 °C.

Solid state ^{31}P NMR spectra was performed using a Bruker Avance III 600 MHz Wide Bore spectrometer equipped with a 4 mm double-resonance probe. The ^{31}P NMR spectra of PDS (0.3) was recorded as follows. Firstly, PDS (0.3) was treated at 130 °C and 10^{-3} Pa for 12 h to remove water. Subsequently, the completely dried sample was adsorbed a known amount of a mixture of TMPO and CH_2Cl_2 in a nitrogen glove box and then CH_2Cl_2 was evaporated at room temperature. To ensure that each pore of the catalyst adsorbed a uniform adsorption of probe molecules, the sample was further thermal treatment at 170 °C for 8 h. Prior to NMR measurement, the sealed sample tube was opened in a dry N_2 glove box. Then, the TMPO-loaded sample was removed into a MAS rotor and sealed by a gas-tight Kel-F cap. For ^{31}P NMR resonance, the Larmor frequency is 600 MHz and the typical π/2 is 4.6 μs. During the ^{31}P MAS NMR spectrum acquisition, the single pulse sequence (equivalent to ca. π/4) is 15 s. The experimental chemical shift is based on $(NH_4)_2HPO_4$ (1.0 ppm) as a standard and the sample spinning frequency is 10 kHz [47,48].

2.3. Catalyst tests

Sorbitol dehydration experiments were performed in a three-necked flask (250 mL), equipped with a magnetic stirrer. The reactor was heated by an electric heating jacket. A certain amount of sorbitol powder was added into the reactor and heated to the reaction temperature under a stirring speed of 1200 rpm. Then, a certain amount of catalyst was added to the reaction system (the time was recorded as t = 0) and the mixture was stirred for the desired time at 0.3 bar. After that, the appropriate amount of reaction product was removed and cooled to room temperature and diluted with deionized water. The insoluble was separated from the sample with an 0.22 μm organic phase needle filter (for HPLC). For comparison, blank tests with addition of only PDVB and no catalyst were also carried out. All experiments were repeated at least twice and the results showed that the relative error was less than ± 1%.

The products were analyzed by a high performance liquid chromatography (HPLC, LC-10Avp) equipped with an Aminex® HPX-87H column (7.8 × 300 mm, 9.0 μm) and differential refraction detector (RID-10 A) using 0.005 M H_2SO_4 solution as mobile phase at a flow rate of 0.6 mL/min. The column temperature was maintained at 60 °C throughout the analysis. However, substances with similar chemical structures such as 1,4-sorbitan and 3,6-sorbitan are co-eluted in a single peak [41]. While trace amounts of 2,5-mannitan and 1,5-sorbitan are not always well separated from the peak of 1,4-sorbitan. So we decide to integrate the peaks of the above single dehydrated products to obtain the total sorbitans quantity, and the result was shown in Table 2 as "Sorbitans Selectivity". The calculated method is according to the reported method of previous researchers [17,29,36,41]. Sorbitol and isosorbide use their respective response factors, and other single dehydrated products use the response factor of 1,4-sorbitan. Unknowns and insolubles (polymer/humins) were calculated from the difference between the initial amount of sorbitol and all products obtained by HPLC.

The sorbitol conversion ($C_{Sorbitol}$), isosorbide selectivity ($S_{Isosorbide}$), sorbitan selectivity ($S_{Sorbitan}$) and yield ($Y_{Isosorbide}$) were calculated by the following equation:

$$C_{Sorbitol}\ (\%) = \frac{n_{sorbitol\ initial} - n_{sorbitol\ in\ product}}{n_{sorbitol\ initial}} \times 100 \quad (1)$$

$$S_{Isosorbide}\ (\%) = \frac{n_{isosorbide}}{n_{sorbitol\ initial} - n_{sorbitol\ in\ product}} \times 100 \quad (2)$$

$$Y_{Isosorbide}\ (\%) = \frac{C_{Sorbitol} \times S_{Isosorbide}}{100} \quad (3)$$

$$S_{Sorbitan}\ (\%) = \frac{n_{sorbitan}}{n_{sorbitol\ initial} - n_{sorbitol\ in\ product}} \times 100 \quad (4)$$

In which, $n_{sorbitol\ initial}$ is the initial molar concentration of sorbital, mol/L. $n_{sorbitol\ in\ product}$ is the molar concentration of sorbitol in the product, mol/L. $n_{isosorbide}$ is the molar concentration of isosorbide in the product, mol/L. $n_{sorbitan}$ is the molar concentration of sorbitan in the product, mol/L.

The Turn Over Frequency (TOF) values were calculated by the following equation:

$$TOF = \frac{n_{sorbitol} \times C_{sorbitol}}{m_{cat} \times N_{acid\ site} \times t} \quad (5)$$

In which, $n_{sorbitol}$ is the molar mass of sorbitol, mol. $C_{sorbitol}$ is the conversion of sorbitol (< 20%). m_{cat} is the mass of catalyst, g. $N_{acid\ site}$ is the concentration of acid sites measured by CHNS, mmol/g. The reaction time was presented by t, h.

3. Results and discussion

3.1. Catalyst characterization

Scheme S1 shows the synthesis of catalyst PDS (x). By using AIBN as an initiator, sodium p-styrenesulfonate and DVB were polymerized substantially to obtain a sodium type polymer precursor. Thereafter, the precursor was ion-exchanged with sulfuric acid to obtain the sulfonic acid functionalized polymer. A series of PDS (x) catalysts were prepared by varying the content of sodium styrene sulfonate, and named as PDS (x) (x = 0.025, 0.07, 0.1, 0.2, 0.3, 0.32 and 0.4), in which x stands for the initial molar ratio of SPSS and DVB.

As shown in Fig. 1A, all samples show typical type-IV isotherms with a H4 hysteresis loop at the high relative pressure region according to the IUPAC classification, which indicates the presence of mesoporous structure [49]. The PDS (x) catalysts show a relatively wide pore size distribution (Fig. 1B). It is well established that the pore size distribution of the catalyst is influenced by the concentration of acid sites. As expected, enhancing the ratio of sulfonic acid groups (from 0 to 0.4), the BET surface area, pore volume and average pore diameter of PDS (x) decrease gradually (Table 1, Entry 2–9). The specific surface area of hypercrosslinked PDS (x) is still much higher than that of macroporous resins (Table S1) [38]. The decreased pore volume can be attributed to the increasing of the amount of sulfonic acid groups grafted in the pores [50]. However, due to the solubility of sodium styrene sulfonate in DVB, the amount of sulfonic acid groups grafted was limited, i.e. the pore volume and pore size of PDS (0.32) and PDS (0.4) are very similar (Table 1, Entry 7 and 8).

Table 1 illustrates the results of elemental analysis and acid-base titration of the PDS (x) catalysts. As the amount of grafted sulfonic acid groups increases, both the S concentration and the amount of the acid sites increase (Table 1, Entry 1–8). Remarkably, S concentration and the acid sites are in good accordance with each other i.e. by changing the amount of sodium p-styrene sulfonate, the acid sites of the catalyst can be accurately regulated.

In order to determine the acid site type, the pyridine infrared (Py-IR) spectrum [51] of PDS (0.1), PDS (0.3) and PDS (0.4) were collected (Fig. S1). The characteristic peak of Brønsted acid site at 1545 cm^{-1} was observed, whose area gradually increases as the grafting amount of the sulfonic acid group increases, in good agreement with the acid-base titration and elemental analysis. It is worth noting that the

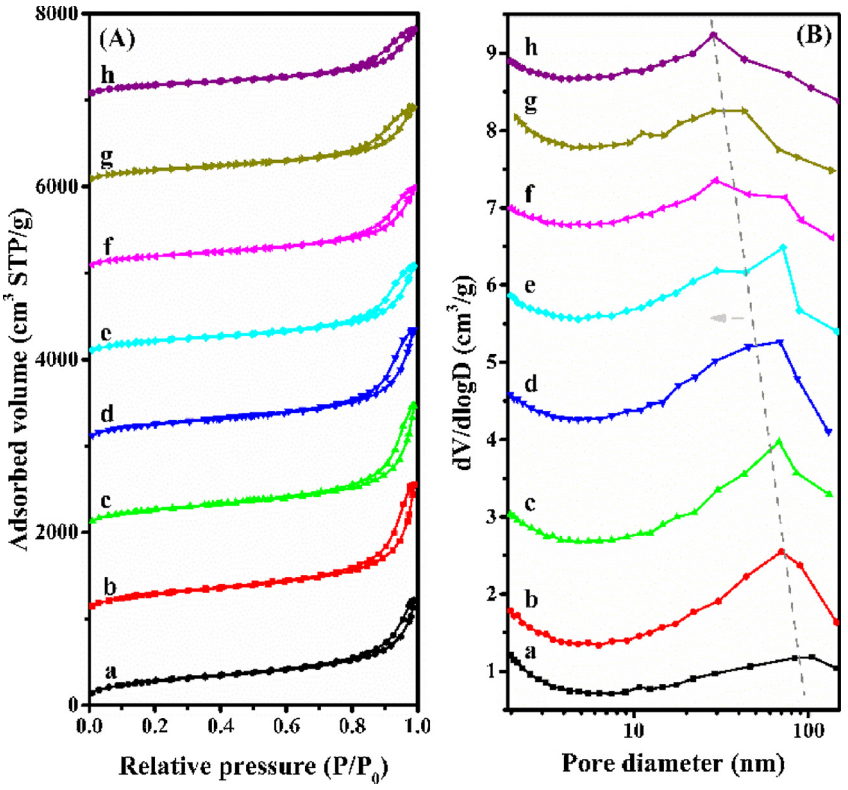

Fig. 1. (A) N_2 sorption isotherms and (B) pore size distribution curves of (a) PDVB, (b) PDS (0.025), (c) PDS (0.07), (d) PDS (0.1), (e) PDS (0.2), (f) PDS (0.3), (g) PDS (0.32), (h) PDS (0.4).

characteristic peak of Lewis acid site (1450 cm^{-1}) did not appear for all catalysts, indicating that the PDS (x) catalyst is a Brønsted acid catalyst.

As shown in Fig. S2, the XRD pattern of the precursor PDVB and PDS (x) samples have broad Bragg reflection, indicating the amorphous structure of catalysts both before and after grafting of the sulfonic acid group.

Fig. 2 presents the SEM and TEM images of PDVB and PDS (0.3). The PDVB presents irregular fluffy coral-shaped morphology (Fig. 2A), while PDS (0.3) shows a loose spongy structure (Fig. 2B). The samples consisted of particles with rich pores (10–100 nm), which may lead to the large specific surface area. The abundant wormhole-like morphology indicates the highly cross linked framework (Fig. 2C and D) which are in good accordance with the BET and XRD results.

To illustrate the hydrophilicity/hydrophobicity of the PDVB and PDS (x) catalyst surface, the water contact-angle was measured (Fig. 3). The water contact angle of PDVB (Fig. 3A) is up to 150°, indicating the superhydrophobic structure [46]. However, as the amount of grafted sulfonic acid groups increased (x = 0.025–0.4), the hydrophobic angles tend to decrease slightly from 157° to 140° (Fig. 3B–H). Due to the superhydrophobicity of the PDS (x) catalyst, the water produced by the dehydration reaction can be removed in time and thus the catalytic activity can be promoted.

To further explore the hydrophobicity of the PDS (x) catalyst, the adsorption behaviors of water vapour were carried out (Fig. S3). Interestingly, the PDS (x) catalyst shows stronger hydrophobicity than Amberlyst-15, i.e. although the amount of water uptake increased with the increased degree of sulphonation, it was always lower than that of Amberlyst-15. Liu et al. also reported the similar results [50]. The

Table 1
Textural properties and acidic parameters of PDS (x).

Entry	Catalyst support	SPSS:DVB (mol/mol)	S content (mmol/g)[a]	Acid sites (mmol/g)[b]	S_{BET} (m^2/g)[c]	V_p (cm^3/g)[d]	D_p (nm)[e]
1	PDVB	0:1	0.00	0	1008	1.88	9.14
2	PDS(0.025)	0.025:1	0.25	0.23	1039	2.4	10.82
3	PDS(0.07)	0.07:1	0.37	0.45	951	2.27	10.95
4	PDS(0.1)	0.1:1	0.60	0.67	910	2.08	10.25
5	PDS(0.2)	0.2:1	1.06	1.15	774	1.67	9.75
6	PDS(0.3)	0.3:1	1.38	1.53	715	1.52	9.49
7	PDS(0.32)	0.32:1	1.46	1.59	694	1.42	9.07
8	PDS(0.4)	0.4:1	1.72	1.81	635	1.27	9.08
9	PDS(0.3)[f]	0.3:1	1.28	1.32	244	0.40	9.78

[a] Measured by elemental analysis.
[b] Measured by acid-base titration.
[c] BET surface area.
[d] Total pore volume.
[e] Average pore size.
[f] Recycled five times.

Table 2
Performances of various catalysts for sorbitol dehydration to isosorbide.[a]

Entry	Catalyst	Conv.[b] (%)	Yield[b] (%)	Selectivity[b] (%)			TOF[c] (h^{-1})
				Isosorbide	Sorbitans	Others[d]	
1	None	0.89	–	–	–	100	–
2	PDVB	0.98	–	–	–	100	–
3	PDS(0.025)	79.1	11.4	14.4	84.6	1.0	85
4	PDS(0.07)	90.6	26.9	29.7	69.4	0.9	135
5	PDS(0.1)	96.0	43.4	45.2	54.0	0.8	222
6	PDS(0.2)	95.5	71.0	74.3	24.7	1.0	129
7	PDS(0.3)	94.1	81.7	86.8	11.1	2.1	110
8	PDS(0.32)	94.7	78.9	83.3	14.4	2.3	102
9	PDS(0.4)	95.2	82.2	86.3	10.6	3.1	80
10	PDS(0.3)[e]	95.4	73.5	77.0	21.2	1.8	115
11	H_2SO_4	94.0	81.1	86.3	9.5	4.2	143

[a] Reaction conditions: sorbitol 25 g, catalyst 2 wt%, 150 °C, 0.3 bar, 12 h.
[b] Determined by HPLC with an Aminex® HPX-87H column using 0.005 M H_2SO_4 solution as mobile phase with the flow rate 0.6 mL/min at 60 °C.
[c] Turnover frequency (TOF, h^{-1}).
[d] "Others selectivity" = 100- "isosorbide selectivity"- "sorbitans selectivity".
[e] Recycled for five times.

amount of adsorbed water on these catalysts decreased in the order: Amberlyst-15 > PDS (0.4) > PDS (0.3) ≈ PDS (0.3) 5th > PDS (0.1) > PDVB, which is consistent with the water contact-angle tests.

Fig. 4A illustrates the FT-IR spectra of PDVB and PDS (x). The characteristic vibration band at around 1035 cm^{-1} is assigned to the C—S band stretching on the benzene rings. For PDS (x) samples, the bands at 1008, 1125, 1178 cm^{-1} are ascribed to symmetric and asymmetric stretching vibrations of O═S═O of $-SO_3H$. Moreover, the characteristic peaks of C—S and O═S═O gradually increase with the increase of the amount of grafted sulfonic acid groups. These features indicate that the sulfonic acid groups are successfully introduced onto the polymer matrix which are consistent with the results of elemental analysis.

Fig. 4C, 4D and S4 shows the X-ray photoelectron spectroscopy (XPS) results of PDVB and PDS (0.3) samples. Both spectra exhibit the peaks of C and O. The spectrum of PDS (0.3) also shows the peak of S 2p and S 2 s. The peaks at 164.3 eV (S 2p) and 233 eV (S 2 s) belong to the S—O and S═O bonds. For the C 1 s peaks of PDS (0.3) (Fig. 4D), the bands at 286 eV and 284.8 eV can be ascribed to C—S and C—C bonds of sulfonate groups grafted onto the polymer precursors [50,52]. The results of XPS are consistent with the FT-IR results. In addition, the ratio of peak areas of C—S and C—C corresponds well with the results of the elemental analysis (S/C = 0.02173).

To investigate the acid strength of the catalyst, ^{31}P solid-state NMR was measured (Fig. 4B). Two characteristic peaks were found by Gaussian simulation at 80 ppm (40%) and 84 ppm (60%), respectively. According to the research by A. Zheng et al. [48], the PA values (proton affinity value) of 80 ppm and 84 ppm were 263 kcal/mol and 253 kcal/mol, respectively, e.g. PDS (0.3) belongs to strong acid catalyst.

Fig. 5 shows the TG-DTG curves of Amberlyst-15, Nafion, PDVB and PDS (0.3). Three stages of weight loss, at 30–150, 200–400 and 400–600 °C are observed. The initial weight loss (about 3–5%) between

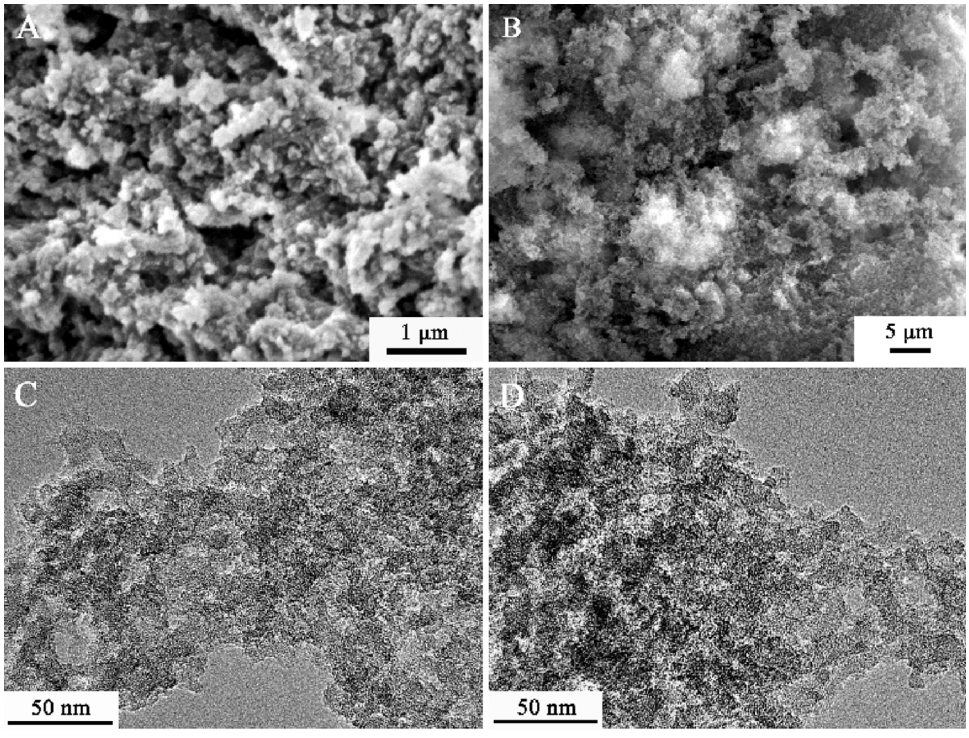

Fig. 2. SEM and TEM images of PDVB (A and C) and PDS (0.3) (B and D).

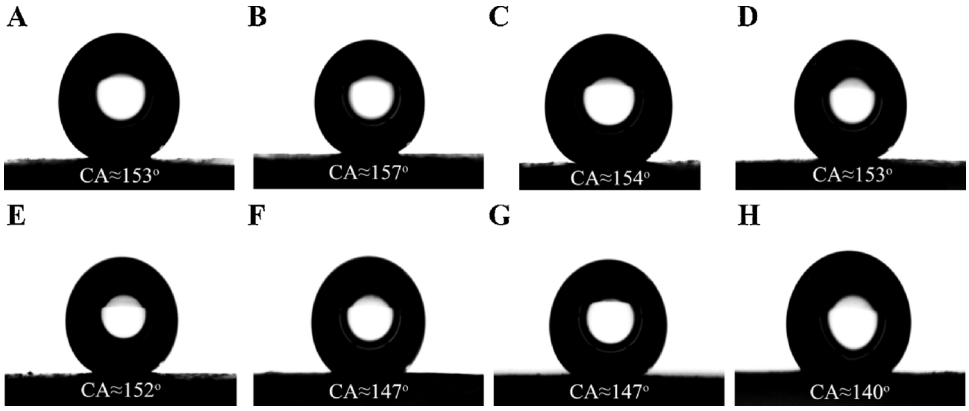

Fig. 3. Water droplet contact angles on (A) PDVB, (B) PDS (0.025), (C) PDS (0.07), (D) PDS (0.1), (E) PDS (0.2), (F) PDS (0.3), (G) PDS (0.32) and (H) PDS (0.4).

30 and 150 °C is due to the desorption of physically adsorbed water in the catalyst surface and pores. The weight loss at 200-400 °C (about 35–40%, except Nafion of 17%) and 400–600 °C (about 55–60%, except Nafion of 81%) is due to the decomposition of the sulfonic acid component and the collapse of polymer structure, respectively. The decomposition temperature of sulfonic groups and polymer structure of PDS (0.3), at 375 °C and 500 °C, are higher than that of Amberlyst-15 (290 and 500 °C), Nafion (340 and 430 °C) and PDVB precursor (330 and 470 °C). Moreover, the final decomposition temperature of PDS (0.3) is similar to PDVB at about 550 °C, reflecting the high thermal stability of the samples. Fig. S5 shows that the TG-DTG curves of other PDS (x) samples are similar to that of PDS (0.3).

3.2. Catalytic performance for the dehydration of sorbitol to isosorbide

To test the catalytic performance of PDS (x) catalysts, a series of evaluation experiments was carried out. Water is unfavorable for the dehydration reaction [53] at low temperature and may affect the catalytic performance of the catalyst. Therefore, in order to quickly remove water from the reaction system, the experiment was carried under vacuum. In addition, to exclude the influence of the evacuation on the reaction results, we also list the catalytic results under ambient conditions (Fig. S6).

The catalytic activities for sorbitol dehydration over various acid catalysts are listed in Table 2. All the reactions were carried out under vacuum (0.3 bar) at 150 °C for 12 h. The product comprises doubly-

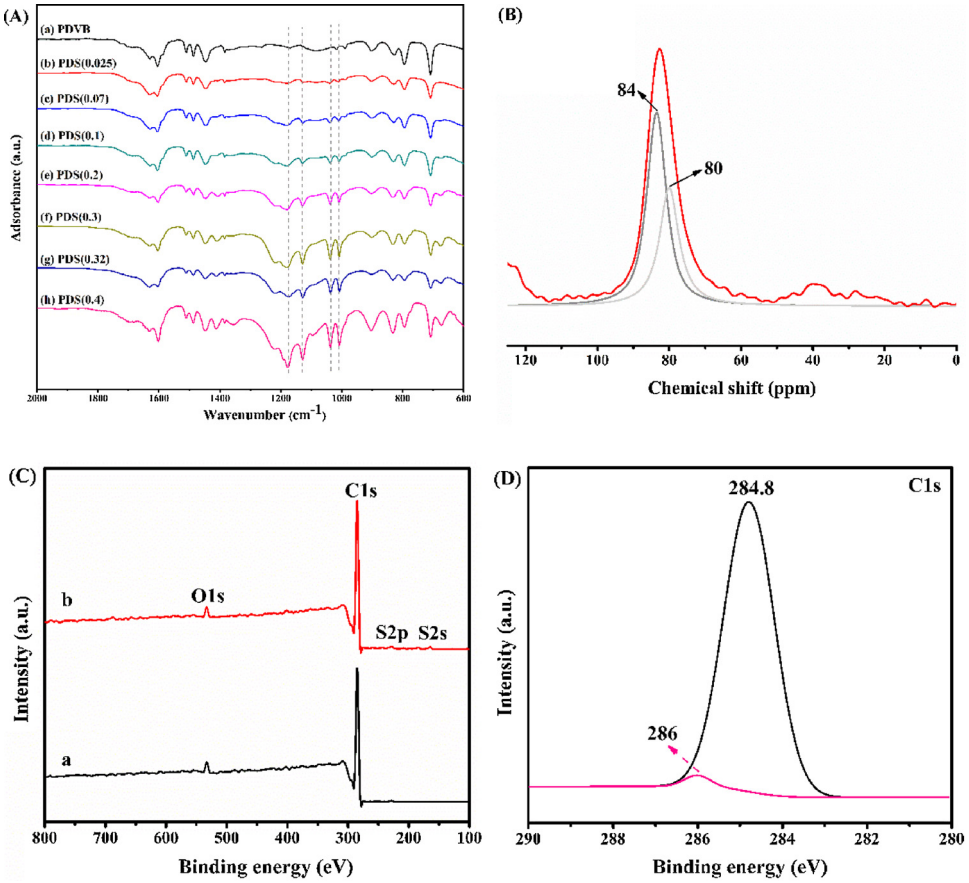

Fig. 4. (A) FT-IR of (a) PDVB, (b) PDS (0.025), (c) PDS (0.07), (d) PDS (0.1), (e) PDS (0.2), (f) PDS (0.3), (g) PDS (0.32) and (h) PDS (0.4); (B) ^{31}P MAS NMR spectra of PDS (0.3) adsorbed TMPO; (C)&(D) XPS measurements of (C) (a) PDVB, (b) PDS (0.3), (D) C 1 s of PDS (0.3).

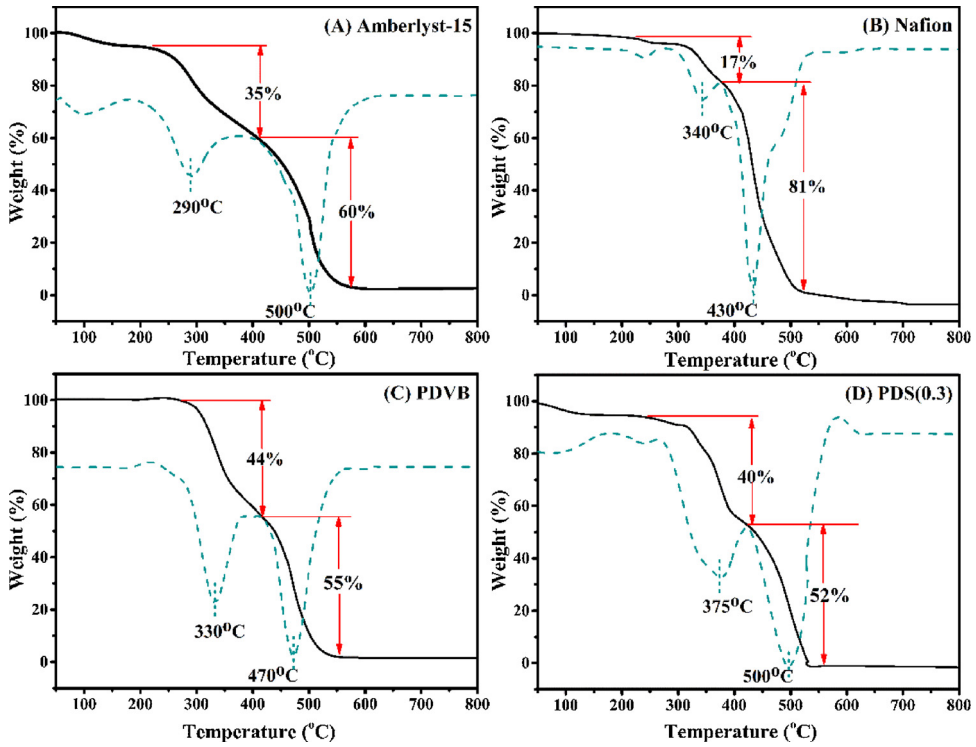

Fig. 5. TG-DTG curves of (A) Amberlyst-15, (B) Nafion, (C) PDVB and (D) PDS (0.3).

dehydrated product isosorbide and the mono-dehydrated products 1,4-anhydrosorbitol, 2,5-anhydrosorbitol, 3,6-anhydrosorbitol, 1,5-anhydrosorbitol. Among them, 1,4-anhydrosorbitol and isosorbide are the main products (> 80%). The calculation error of humins is about ± 3%, which is reasonable for this study [41]. Clearly, sorbitol is hardly dehydrated in the absence of catalyst or over PDVB, even for long reaction time (Table 2, Entry 1, 2). In contrast, PDS (x) samples (Table 2, Entry 3–9) showed excellent catalytic performance. With the increase of the amount of sulfonic acid groups, the conversion of sorbitol (79%–96%) and the yield of isosorbide (11.4%–82.2%) increased gradually.

The turnover frequency values (TOF, h^{-1}) for the sorbitol dehydration reaction were also presented in Table 2. The specific calculation data is listed in Table S2. Notably, under the same reaction conditions, the TOF values of PDS (x) samples first increase and then decrease, reaching the maximum at x = 0.1 (See Section 3.2.1 for the reason.). It is noteworthy that, under the same reaction conditions, the catalytic activity of some catalysts is comparable to that of H_2SO_4.

The PDS (x) catalysts were compared with the previously reported catalytic systems. As shown in Table S3, the catalytic performance of PDS (x) was significantly better than others e.g. the highest yield of isosorbide obtained by PDS (x) is higher than that of other heterogeneous catalytic systems, irrespective of reaction conditions. Moreover, the relatively low reaction temperature in this study not only saves the energy but also prevents the formation of by-products polymers. The excellent catalytic activity of PDS (x) is due to the excellent textural properties, abundant pore structure and superhydrophobicity.

3.2.1. Influence of acid sites concentration, S_{BET} and density

The influence of acid sites concentration on the dehydration reaction of sorbitol is shown in Fig. 6A, where the yield of isosorbide increases with increasing of the acid sites concentration. It is worth noting that when the acid sites concentration of the catalyst increases from 0.25 mmol/g_{cat} (PDS(0.025)) to 1.06 mmol/g_{cat} (PDS (0.2)), the yield of isosorbide increases from 11.4% to 71%. However, when the acid sites concentration increased from 1.38 mmol/g_{cat} (PDS (0.3)) to 1.72 mmol/g_{cat} (PDS (0.4)), the yield of isosorbide only increased from 81.7% to 82.2%. This phenomenon can be well explained by Scheme S2 [54]. For the catalyst with low acid sites concentration (Scheme S2(A)), the acid sites are seperated, and each acid site can interact with sorbitol molecules freely. At the high acid sites concentration (Scheme S2(B)), the close active sites results in the hindrance to sorbitol molecules that lead to less adsorbed feed. This is also the reason why the TOF value of the PDS (x) catalyst first increases and then decreases (see below). Therefore, the concentration of acid sites has a great influence on the yield of isosorbide in a certain range i.e. isosorbide yield gradually decreases when the acid sites concentration reaches a critical point [55].

The influence of specific surface area on the yield of isosorbide is studied and the results are shown in Fig. 6B. The specific surface area of the catalyst decreased from 1008 m^2/g to 635 m^2/g as the acid sites amount increased, while the yield of isosorbide increased gradually. The isosorbide yield as a function of the specific surface area is inversely proportional to the trend of the acid sites concentration.

In order to explore the dominant factors affecting the catalytic activity of the catalyst, the relationship between catalyst acid sites density and TOF values is studied (Fig. 6C). With the increase of the density of the acid sites, the TOF value of PDS (x) increases and then decreases, which implies that both the amount of acid sites and specific surface area have an effect on the catalytic activity. The TOF values of PDS (0.07) and PDS (0.2) are almost the same, but the isosorbide yield of PDS (0.2) is much higher than that of PDS (0.07), indicating that the amount of acid sites is the key factor.

3.2.2. Influence of reaction conditions

In order to study the catalytic performance of PDS (x), the effects of reaction conditions, including the amount of grafted sulfonic acid (0–0.4), temperature (130–170 °C), catalyst amount (0.4–2 wt%) and reaction time (2–24 h) on the reaction were investigated (Fig. 7).

It can be seen from Fig. 7A that as the molar ratio increase, the yield of isosorbide increase from 27% to 87% e.g. more acidic sites favor the reaction. However, high more acidic sites may lead to decreased pore

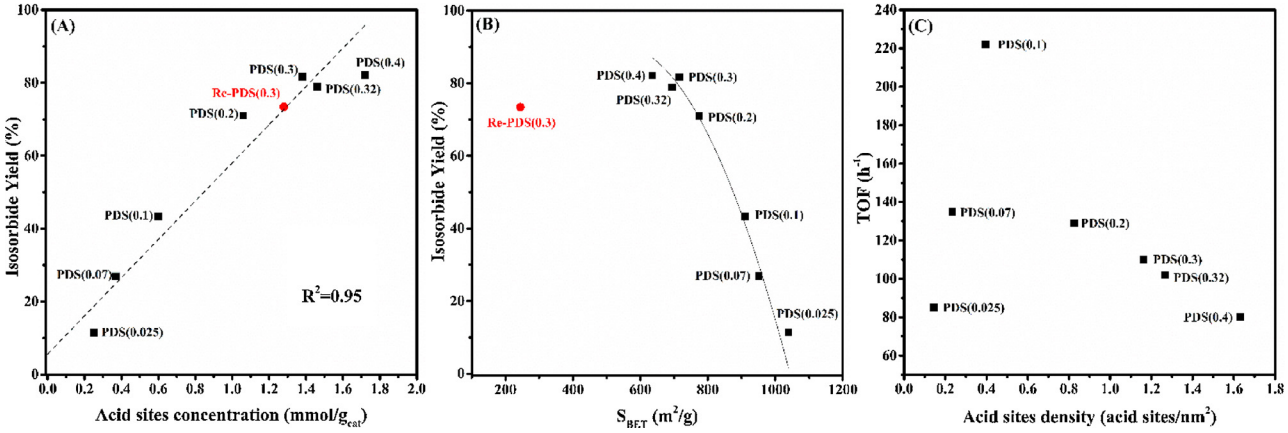

Fig. 6. (A) Isosorbide yield over PDS (x) catalysts as functions of acid sites concentration expressed as mmol/g_{cat}; (B) Influence of S_{BET} on the yield of isosorbide; (C) TOF values over PDS (x) catalysts as functions of acid sites density expressed as acid sites/nm^2.

size and specific surface area, which in turn limits the improvement of catalytic performance. The PDS (0.3) can achieve the highest yield in the shortest time.

With the temperature increased from 130 °C to 150 °C, the isosorbide selectivity increased from 25% to 87% (Fig. 7B), which indicating 1,4-anhydrosorbitol is difficult to further dehydrate to form isosorbide at low temperature. Therefore, raising the temperature is beneficial for increasing the yield of isosorbide. However, higher temperature can lead to the formation of humins/ polymers.

Fig. 7C shows the effect of catalyst dosages on the reaction. As the amount of catalyst increased from 0.4 wt% to 2 wt%, the yield of isosorbide increased from 26% to 82%. In addition, the reaction can reach the equilibrium in a short period of time (12 h) when the mass ratio of catalyst and the sorbitol is 2 wt%.

With the extension of the reaction time (2–24 h) (Fig. 7D), the conversion of sorbitol is almost unchanged (94%) while the selectivity (42–92%) and the yield (40–86%) of isosorbide increased gradually. Because of the extended time, 1,4- anhydrosorbitol can be converted to isosorbide as much as possible.

From the results, it can be concluded that the optimum reaction conditions for the PDS (0.3) catalyst were catalyst/sorbitol = 2 wt%, 0.3 bar, 150 °C, 12 h.

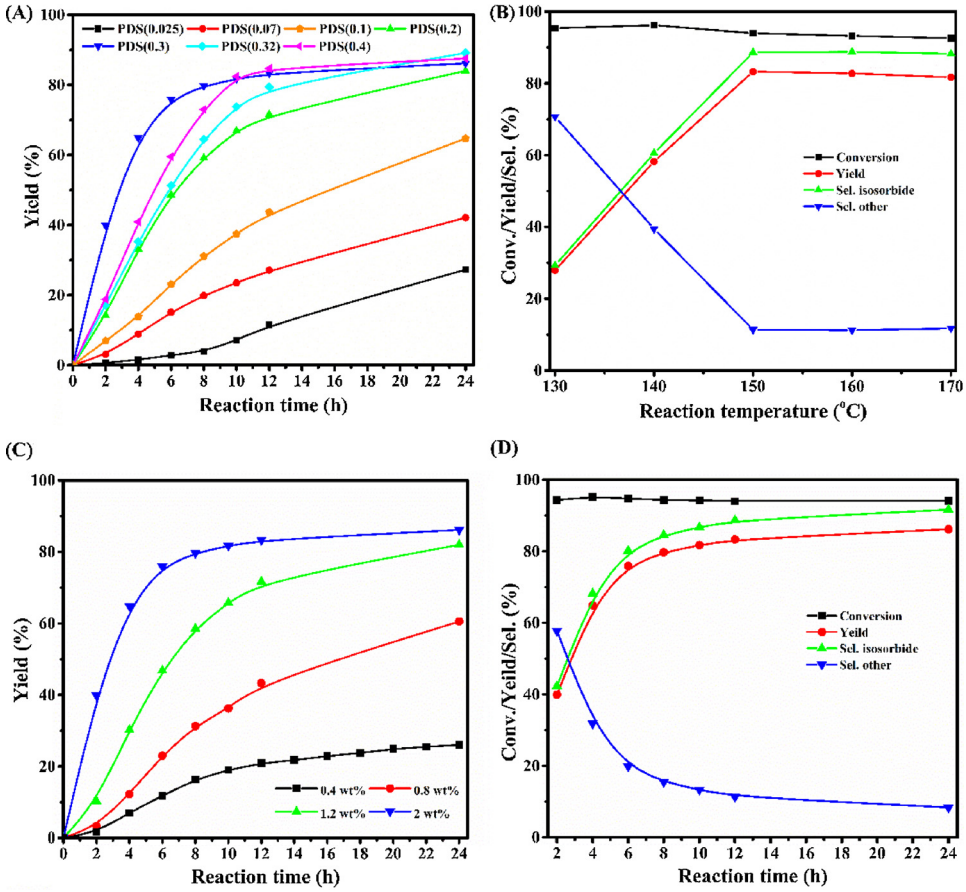

Fig. 7. Influences of (A) reaction time, (B) reaction temperature (12 h), (C) catalyst dosage, (D) reaction time conversion, yield and selectivity over PDS (0.3) catalyst.

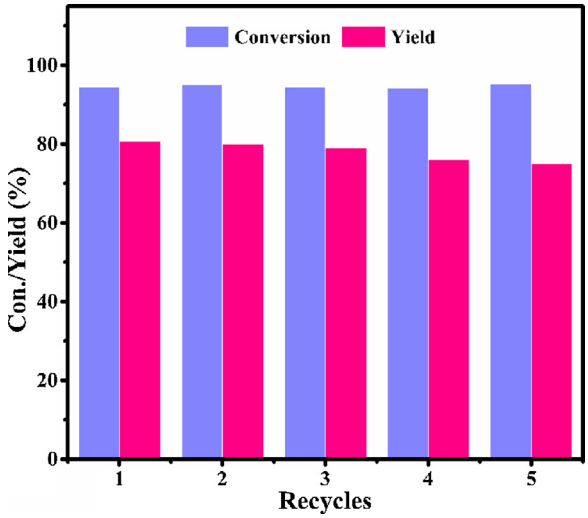

Fig. 8. Reusability of PDS (0.3) for sorbitol dehydration to isosorbide. Reaction conditions: catalyst/sorbitol = 2 wt%, 0.3 bar, 150 °C, 12 h.

3.2.3. Catalyst reusability

Catalyst reusability tests are carried out for PDS (0.3) under the same reaction conditions. The used catalyst PDS (0.3) was filtered, washed by 1,4-dioxane and deionized water for five times, dried at 80 °C for 3 h. Subsequently, the catalyst was activated in 0.1 M H_2SO_4 for 4 h, neutralized with deionized water and dried at 80 °C for 3 h. Finally, the regenerated catalyst is used for the next recycle without adding any fresh catalyst. As shown in Fig. 8 (& Table 2, Entry 10), no significant deactivation are observed even after five runs which is still higher than the conventional solid acid catalysts (Table S3).

In order to determine the state of the recycled catalyst, regenerated catalysts are characterized. As shown in Table 1 (Entry 6 and 9), the results of elemental analysis and acid-base titration show that the acidity of the recycled catalyst did not decrease significantly (from 1.38 mmol/g to 1.28 mmol/g) after five runs. The FT-IR spectra (Fig. S8) show that the characteristic peaks of the recycled catalyst can still be compared with the fresh catalyst which indicates the stable structure of PDS (x). Notably, as shown in Fig. S3, the amount of water absorbed by the PDS (0.3) 5th catalyst is basically the same as that of the fresh catalyst, which can also prove the excellent stability of PDS (0.3). The catalyst still keeps the mesoporous structure (Fig. S7). As shown in Fig. 6A, the relationship between the acid sites concentration and isosorbide yield of the reused PDS (0.3) (Re-PDS (0.3)) is in accordance with that of the fresh catalyst. Although the specific surface area of Re-PDS (0.3) is reduced (Fig. 6B), the activity of the catalyst is still high, further confirming that the acid sites concentration is the main influence factor of the catalyst activity. The high recycle stability may be due to the complete polymer backbone and stable sulfonic acid groups.

3.3. Insight into the reaction of sorbitol to isosorbide

The reaction mechanism is the basis of catalyst design. According to the study of M. Yabushita et al., the most likely mechanism for the dehydration reaction of sorbitol is the S_N2 reaction [56]. Scheme 1 shows the proposed reaction mechanism for Brønsted acid catalyzed dehydration of sorbitol. Firstly, the primary hydroxyl group at position C1 is protonated and then cyclized with a hydroxyl group at the C4 position to remove a molecule of water forming 1,4-sorbitan [34,41]. Thereafter, the hydroxyl group at the C6 position is protonated and attacked by the OH of C3 to produce isosorbide. The dehydration of hydroxyl groups at the C3 and C6 sites might occur in the first step while which is kinetics unfavorable [57]. 2, 5-mannitan and 1, 5-sorbitan may also be formed as by-product which cannot further dehydration to produce isosorbide [14,56]. In addition, sorbitol or other dehydrated products may degrade or polymerize during the reaction, forming the “humins” [18]. According to the above mechanism, a solid acid catalyst with high acidic sites concentration and strong acid strength may have better catalytic performance for the reaction i.e. higher proton concentration increases the probability of sorbitol molecules activated by the acid sites which is consistent with the conclusion of Yamaguchi et al. [14]. However, A. Cubo et al. also pointed out that the effect of acid concentration on the dehydration reaction of the first step (sorbitol to sorbitan) and the second step (sorbitan to isosorbide) is opposite [42], i.e. excessively acid sites result in the simultaneous activation of terminal hydroxyl groups, and the competition of the acid sites reduces the catalytic efficiency. In addition, Yabushita et al. found that the interaction between sulfuric acid and sorbitan is weaker than that with sorbitol [9], which should be applicable to solid acid catalysts as well. By increasing the acidic sites concentration, the interaction between sorbitan and acidic groups can be enhanced [58]. Therefore, the proper acid density is crucial for the high yield of isosorbide. In this study, the acidic sites concentration of PDS (0.3) is most suitable for the sorbitol dehydration reaction.

Another possible explanation for the better activity of PDS (0.3) is the superhydrophobic surface properties. As is well known, the heterogeneous catalytic process can be divided into five steps: adsorption of the reactants, diffusion, conversion, diffusion and desorption of the product (Scheme S3). The main factors affecting catalytic performance are selective adsorption, adsorption mode, diffusion efficiency and active sites, and the first three factors are all controlled by the nature of the support. For the sorbitol dehydration reaction, the hydrophobicity of the support facilitates the smooth entry and exit of the reactants and products, and accelerates the reaction speed from the physical process. From the consideration of the chemical reaction, water has lone pairs of electrons, so it can act as a Lewis base and may compete with the reactants for active sites [53,59]. Moreover, water may also form hydrated protons (H_3O^+-SO_3^-) with the sulfonic acid groups on the inner/ outer surfaces of the catalysts, which may prevent the accessibility of sorbitol molecules [60]. The hydrophobicity of the PDS (0.3) catalyst can remove the water produced by the reaction from the catalyst surface as soon as possible, leading to more exposed active center to the reaction system, thereby resulting in an efficient catalytic performance. In conclusion, the proper acid sites concentration and hydrophobicity of PDS (0.3) lead to its excellent catalytic activity.

4. Conclusions

In summary, the effect of acid sites concentration on the dehydration of sorbitol was studied systematically. PDS (x) catalysts have been demonstrated to catalyze the dehydration of sorbitol to isosorbide with excellent yield under milder conditions is better than that of the traditional heterogeneous acid catalyst. The optimal isosorbide yield was 81.7% obtained by PDS (0.3) at 150 °C for 12 h.

Based on the analysis of the above experimental results, the following conclusions can be drawn:

1) Compared with traditional heterogeneous acid catalysts, PDS (x) has larger specific surface area, higher acidic sites concentration and superhydrophobicity. These properties provide the necessary conditions for efficient catalytic dehydration of sorbitol to isosorbide.
2) The effect of acid sites concentration on the dehydration reaction of sorbitol is more critical when compared with the specific surface area.
3) An insight understanding of the reaction process revealed that PDS (0.3) can catalyze the sorbitol dehydration reaction more efficiently, mainly because both the diffusion process and the chemical kinetics process.

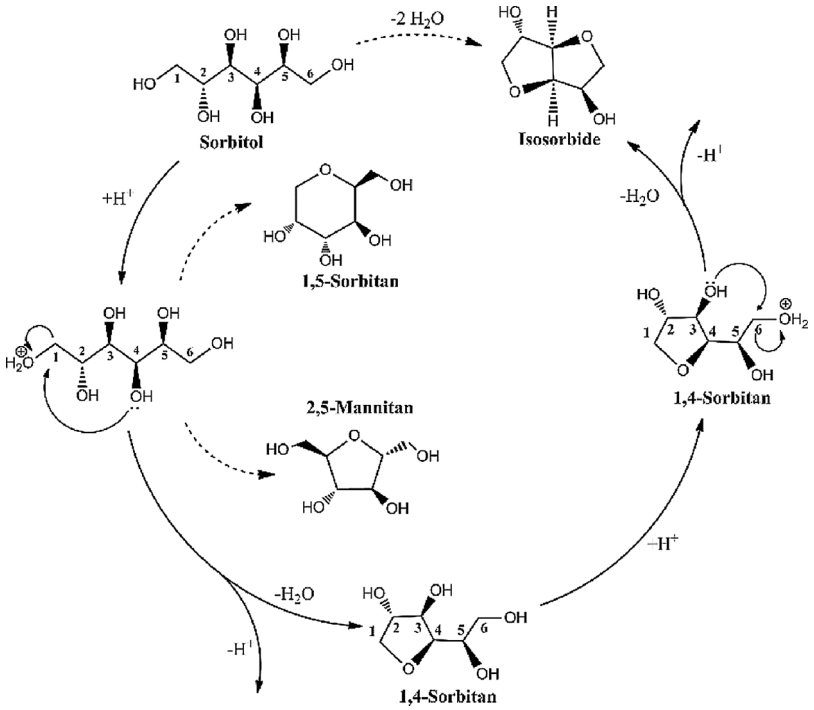

Scheme 1. Proposed reaction mechanism for Brønsted acid catalyzed dehydration of sorbitol.

Acknowledgements

The authors gratefully acknowledge the financial support from the Natural Science Foundation of Shanxi Province, China (No. 201601D102006), the Science Foundation for Young Scientists of Shanxi Province, China (No. 201701D221052), the National Natural Science Foundation of China (21776294), the Key Science and Technology Program of Shanxi Province, China (MD2014-09, MD2014-10) and the Independent Research Project of the State Key Laboratory of Coal Conversion (2018BWZ002).

Appendix A. Supplementary data

Supplementary material related to this article can be found, in the online version, at doi: https://doi.org/10.1016/j.apcatb.2018.08.036.

References

[1] I.A. Telleria, J. Requies, M.B. Güemez, P.L. Arias, Appl. Catal. B: Environ. 115–116 (2012) 169–178.
[2] L. Hu, L. Lin, Z. Wu, S. Zhou, S. Liu, Appl. Catal. B: Environ. 174–175 (2015) 225–243.
[3] L.S. Ribeiro, J.J. Delgado, J.J.M. Órfão, M.F.R. Pereira, Appl. Catal. B: Environ. 217 (2017) 265–274.
[4] P.A. Lazaridis, S.A. Karakoulia, C. Teodorescu, N. Apostol, D. Macovei, A. Panteli, A. Delimitis, S.M. Coman, V.I. Parvulescu, K.S. Triantafyllidis, Appl. Catal. B: Environ. 214 (2017) 1–14.
[5] T. Werpy, G. Petersen, Top Value Added Chemicals From Biomass Volume I-Results of Screening for Potential Candidates From Sugars and Synthesis Gas, U.S. Department of Energy, America, 2004.
[6] J.J. Bozell, G.R. Petersen, Green Chem. 12 (2010) 539–554.
[7] S.P. Collins, P.D. Levy, J.L. Martindale, M.E. Dunlap, A.B. Storrow, P.S. Pang, N.M. Albert, G.M. Felker, G.J. Fermann, G.C. Fonarow, M.M. Givertz, J.E. Hollander, D.E. Lanfear, D.J. Lenihan, J.M. Lindenfeld, W.F. Peacock, D.B. Sawyer, J.R. Teerlink, J. Butler, Acad. Emerg. Med. 23 (2016) 922–931.
[8] B. Yin, M. Hakkarainen, J. Appl. Polym. Sci. 119 (2011) 2400–2407.
[9] H. Yokoyama, H. Kobayashi, J.Y. Hasegawa, A. Fukuoka, ACS Catal. 7 (2017) 4828–4834.
[10] J. Li, W. Buijs, R.J. Berger, J.A. Moulijn, M. Makkee, Catal. Sci. Technol. 4 (2014) 152–163.
[11] J. Li, A. Spina, J.A. Moulijn, M. Makkee, Catal. Sci. Technol. 3 (2013) 1540–1546.
[12] F. Liu, K.D.O. Vigier, M.P. Titus, Y. Pouilloux, J.M. Clacens, F. Decampo, F. Jérôme, Green Chem. 15 (2013) 901–909.
[13] A. Yamaguchi, N. Muramatsu, N. Mimura, M. Shirai, O. Sato, Phys. Chem. Chem. Phys. 19 (2017) 2714–2722.
[14] A. Yamaguchi, N. Hiyoshi, O. Sato, M. Shirai, Green Chem. 13 (2011) 873–881.
[15] J. Muller, U. Hoffmann, US Patent #1757468 (1930).
[16] K. Stensrud, S. Howard, A. Sanborn, E. Hagberg, WO Patent App. PCT/ US, 2014/ 070050 (2015).
[17] A.A. Dabbawala, D.K. Mishra, G.W. Huber, J.S. Hwang, Appl. Catal. A Gen. 492 (2015) 252–261.
[18] G. Flèche, M. Huchette, Starch 38 (1986) 26–30.
[19] C. Dussenne, T. Delaunay, V. Wiatz, H. Wyart, I. Suisse, M. Sauthier, Green Chem. 19 (2017) 5332–5344.
[20] M. Kurszewska, E. Skorupowa, J. Madaj, A. Konitz, W. Wojnowski, A. Wiśniewski, Carbohydr. Res. 337 (2002) 1261–1268.
[21] C. García-Sancho, R. Moreno-Tost, J.M. Mérida-Robles, J. Santamaría-González, A. Jiménez-López, P. Maireles-Torres, Appl. Catal. B: Environ. 108–109 (2011) 161–167.
[22] C. Antonetti, M. Mellonic, D. Licursi, S. Fulignati, E. Ribechini, S. Rivas, J.C. Parajó, F. Cavani, A.M.R. Galletti, Appl. Catal. B: Environ. 206 (2017) 364–377.
[23] I. Sádaba, M. Ojeda, R. Mariscal, M.L. Granados, Appl. Catal. B: Environ. 150–151 (2014) 421–431.
[24] J. Ni, D. Rooney, F.C. Meunier, Appl. Catal. B: Environ. 97 (2010) 269–275.
[25] Y.H. Guo, K.X. Li, X.D. Yu, J.H. Clark, Appl. Catal. B: Environ. 81 (2008) 182–191.
[26] H. Kobayashi, H. Yokoyama, B. Feng, A. Fukuoka, Green Chem. 17 (2015) 2732–2735.
[27] R. Otomo, T. Yokoi, T. Tatsumi, Appl. Catal. A Gen. 505 (2015) 28–35.
[28] H. Li, D. Yu, Y. Hu, P. Sun, J. Xia, H. Huang, Carbon 48 (2010) 4547–4555.
[29] M. Gu, D. Yu, H. Zhang, P. Sun, H. Huang, Catal. Lett. 133 (2009) 214–220.
[30] O.A. Rusu, W.F. Hoelderich, H. Wyart, M. Ibert, Appl. Catal. B: Environ. 176–177 (2015) 139–149.
[31] J. Xia, D. Yu, Y. Hu, B. Zou, P. Sun, H. Li, H. Huang, Catal. Commun. 12 (2011) 544–547.
[32] N.A. Khan, D.K. Mishra, I. Ahmed, J.W. Yoon, J.S. Hwang, S.H. Jhung, Appl. Catal. A Gen. 452 (2013) 34–38.
[33] I. Ahmed, N.A. Khan, D.K. Mishra, J.S. Lee, J.S. Hwang, S.H. Jhung, Chem. Eng. J. 93 (2013) 91–95.
[34] A.A. Dabbawala, D.K. Mishra, J.S. Hwang, Catal. Commun. 42 (2013) 1–5.
[35] Z.C. Tang, D.H. Yu, P. Sun, H. Li, H. Huang, Bull. Korean Chem. Soc. 31 (2010) 3679–3683.
[36] X. Zhang, D. Yu, J. Zhao, W. Zhang, Y. Dong, H. Huang, Catal. Commun. 43 (2014) 29–33.
[37] P. Sun, D.H. Yu, Y. Hu, Z.C. Tang, J.J. Xia, H. Li, H. Huang, Korean J. Chem. Eng. 28 (2011) 99–105.
[38] E. Andrijanto, E.A. Dawson, D.R. Brown, Appl. Catal. B: Environ. 115–116 (2012) 261–268.
[39] J. Shi, Y. Shan, Y. Tian, Y. Wan, Y. Zheng, Y. Feng, RSC Adv. 6 (2016) 13514–13521.
[40] M.J.G. Molina, R.M. Tost, J.S. González, P.M. Torres, Appl. Catal. A Gen. 537 (2017) 66–73.
[41] I. Polaert, M.C. Felix, M. Fornasero, S. Marcotte, J.C. Buvat, L. Estel, Chem. Eng. J. 222 (2013) 228–239.

[42] A. Cubo, J. Iglesias, G. Morales, J.A. Melero, J. Moreno, R. Sánchez-Vázquez, Appl. Catal. A Gen. 531 (2017) 151–160.
[43] R.S. Thombal, V.H. Jadhav, Tetrahedron Lett. 57 (2016) 4398–4400.
[44] J. Zhang, L. Wang, F. Liu, X. Meng, J. Mao, F.S. Xiao, Catal. Today 242 (2015) 249–254.
[45] W. Deng, M. Liu, X. Tan, Q. Zhang, Y. Wang, J. Catal. 271 (2010) 22–32.
[46] Y. Zhang, S. Wei, F. Liu, Y. Du, S. Liu, Y. Ji, T. Yokoi, T. Tatsumi, F.S. Xiao, Nano Today 4 (2009) 135–142.
[47] A. Zheng, S.J. Huang, S.B. Liu, F. Deng, Phys. Chem. Chem. Phys. 13 (2011) 14889–14901.
[48] A. Zheng, H. Zhang, X. Lu, S.B. Liu, F. Deng, J. Phys. Chem. B 112 (2008) 4496–4505.
[49] R.V.G.J.A. Melero, G. Morales, Chem. Rev. 106 (2006) 3790–3812.
[50] F. Liu, W. Kong, C. Qi, L. Zhu, F.S. Xiao, ACS Catal. 2 (2012) 565–572.
[51] C.A. Emeis, J. Catal. 141 (1993) 347–354.
[52] C. Kolbeck, M. Killian, F. Maier, N. Paape, P. Wasserscheid, H.P. Steinrück, Langmuir 24 (2008) 9500–9507.
[53] Z. Zhang, J. Song, B. Han, Chem. Rev. 117 (2017) 6834–6880.
[54] Y. Choi, H. Park, Y.S. Yun, J. Yi, ChemSusChem 8 (2015) 974–979.
[55] C. García-Sancho, J.A. Cecilia, J.M. Mérida-Robles, J. Santamaría González, R. Moreno-Tost, A. Infantes-Molinab, P. Maireles-Torres, Appl. Catal. B: Environ. 221 (2018) 158–168.
[56] M. Yabushita, H. Kobayashi, A. Shrotri, K. Hara, S. Ito, A. Fukuoka, B. Chem. Soc. Japan 88 (2015) 996–1002.
[57] M. Shirai, O. Sato, N. Hiyoshi, A. Yamaguchi, J. Chem. Sci. 126 (2014) 395–401.
[58] J.P. Dacquin, H.E. Cross, D.R. Brown, T. Düren, J.J. Williams, A.F. Lee, K. Wilson, Green Chem. 12 (2010) 1383.
[59] H. Tang, N. Li, G. Li, W. Wang, A. Wang, Y. Cong, X. Wang, ACS Sustain. Chem. Eng. 6 (2018) 5645–5652.
[60] V. Trombettoni, D. Lanari, P. Prinsen, R. Luque, A. Marrocchi, L. Vaccaro, Prog. Energy Combust. Sci. 65 (2018) 136–162.